

Low strength of deep San Andreas fault gouge from SAFOD core

David A. Lockner¹, Carolyn Morrow¹, Diane Moore¹ & Stephen Hickman¹

The San Andreas fault accommodates 28–34 mm yr⁻¹ of right lateral motion of the Pacific crustal plate northwestward past the North American plate. In California, the fault is composed of two distinct locked segments that have produced great earthquakes in historical times, separated by a 150-km-long creeping zone. The San Andreas Fault Observatory at Depth (SAFOD) is a scientific borehole located northwest of Parkfield, California, near the southern end of the creeping zone. Core was recovered from across the actively deforming San Andreas fault at a vertical depth of 2.7 km (ref. 1). Here we report laboratory strength measurements of these fault core materials at *in situ* conditions, demonstrating that at this locality and this depth the San Andreas fault is profoundly weak (coefficient of friction, 0.15) owing to the presence of the smectite clay mineral saponite, which is one of the weakest phyllosilicates known. This Mg-rich clay is the low-temperature product of metasomatic reactions between the quartzofeldspathic wall rocks and serpentinite blocks in the fault^{2,3}. These findings provide strong evidence that deformation of the mechanically unusual creeping portions of the San Andreas fault system is controlled by the presence of weak minerals rather than by high fluid pressure or other proposed mechanisms¹. The combination of these measurements of fault core strength with borehole observations^{1,4,5} yields a self-consistent picture of the stress state of the San Andreas fault at the SAFOD site, in which the fault is intrinsically weak in an otherwise strong crust.

SAFOD is a deep scientific borehole that penetrates the San Andreas fault (SAF) at a vertical depth of approximately 2.7 km and is the deepest land-based scientific drilling project to cross a plate-bounding fault^{1,6,7} (see <http://www.earthscope.org> for additional information). During phase 2 drilling in 2005, the basic structure of the SAF was determined (Fig. 1) using borehole logging data¹ and supplementary laboratory studies of the drilling cuttings^{8,9}. At 2.7 km depth, the damage zone associated with the fault is approximately 200 m wide, and two actively creeping strands were identified within it by accumulated deformation of the steel casing in the main borehole¹. These two active shear zones, referred to as the southwest deforming zone (SDZ) and the central deforming zone (CDZ), were primary targets of the phase 3 multilateral core drilling operation in 2007. Approximately 31 m of core were recovered from across the SDZ, CDZ and adjoining damage-zone rocks, including 1.6 m and 2.6 m of highly foliated, incohesive fault gouge associated with the SDZ and CDZ, respectively.

We have completed frictional strength measurements on 25 core samples that span the important lithologic units. Of these, 17 are detrital sedimentary rocks, ranging from fine-grained sandstones to mudstones; representative X-ray diffraction (XRD) patterns are presented in Supplementary Fig. 2. The SDZ and CDZ are represented by four samples apiece. In marked contrast to the adjoining rocks, both foliated gouge zones consist of porphyroclasts of serpentinite and sedimentary rock dispersed in a matrix of Mg-rich clays¹⁰ (Supplementary Fig. 3). XRD patterns of the CDZ were dominated by saponite (estimated to be greater than 60% from petrographic analysis) with some quartz and calcite. The SDZ gouge was composed primarily of saponite + corrensite with some quartz and feldspars (corrensite is a

regularly interlayered chlorite-saponite clay). The porphyroclasts are also partly altered to Mg-rich clays³. The two gouge zones are interpreted to be the product of shearing-enhanced metasomatic reactions between serpentinite, tectonically entrained within the fault, and adjoining sedimentary rocks^{2,3}.

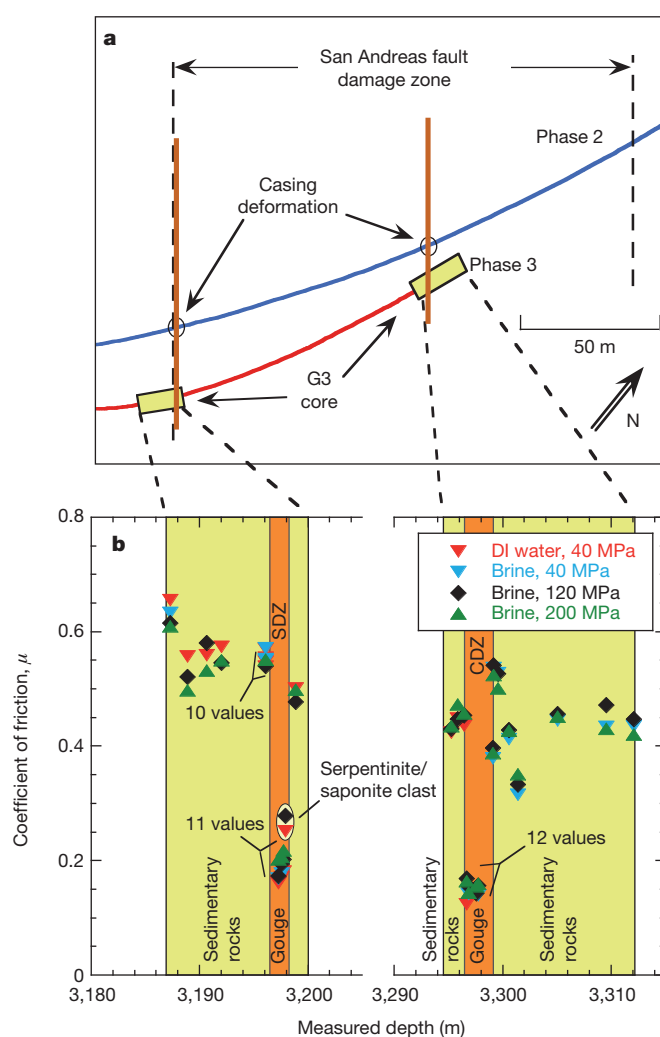


Figure 1 | Location and strengths of SAFOD core samples. **a**, Map view of SAF damage zone and SAFOD boreholes from phase 2 (blue) (indicating actively deforming casing) and phase 3 Hole G (red) with location of recovered core (yellow) at approximately 2.7 km vertical depth. Active deformation zones are shown in orange. **b**, Frictional strength of core samples plotted versus measured depth along Hole G (at sliding rate $V = 1.15 \mu\text{m s}^{-1}$). Active fault traces SDZ (3,196.4–3,198.1 m measured depth) and CDZ (3,296.6–3,299.1 m) have notably low strength. A few samples were tested with deionized (DI) water. Extrapolation to SAF plate rate reduces shear zone strength to $\mu \approx 0.15$.

¹US Geological Survey, Menlo Park, California 94025, USA.

Sample strength is reported as coefficient of friction $\mu = \tau/\bar{\sigma}_n$, where τ and $\bar{\sigma}_n$ are respectively shear stress and effective normal stress on the test faults; we estimate *in situ* $\bar{\sigma}_n$ to be ~ 122 MPa (see below). Here, $\bar{\sigma}_n = \sigma_n - p$, where σ_n is normal stress and p is pore pressure. Representative strength tests are plotted in Fig. 2. Frictional strength was compiled from all deformation tests at 9.8–10.4 mm fault-parallel slip and sliding rate $V = 1.15 \mu\text{m s}^{-1}$. As shown in Fig. 2, nearly all time- and slip-dependent strengthening had ended by 10 mm slip, so that residual strength is reasonably represented by this value. Residual strength refers to the stable strength of the test sample once fully developed shear flow is established. Because control parameters—including σ_n , p , V and pore fluid composition—are duplicated in the tests, variations in μ are attributed to mineralogical differences between samples. Samples outside the two shear zones show a gradual weakening trend, from $\mu \approx 0.6$ on the southwestern side to $\mu \approx 0.4$ on the northeastern side. This trend reflects a compositional change from more quartz-rich sandstone and siltstone on the southwestern side to more phyllosilicate-rich mudstones to the northeast (Supplementary Fig. 2). The SDZ marks the southwestern boundary of the damage zone, so that the samples with the highest residual strength reside outside the damage zone ($\mu \approx 0.50\text{--}0.65$).

The most significant strength observation is the abrupt decrease in μ within the two actively deforming shear zones. All residual strength measurements of the foliated gouge (at 10.4 mm slip) yield $\mu \leq 0.21$; the weakest sample has a strength of $\mu = 0.13$ (Fig. 1). A partly altered serpentinite porphyroclast from the SDZ has a strength of $\mu \approx 0.26$ and apparently survived by weaker matrix material flowing around it. The very low measured strengths are attributed to the abundance of the extremely weak mineral saponite ($\mu \approx 0.05$) (Fig. 2). Petrographic analysis indicates a saponite volume fraction of 60–65% in the foliated gouge matrix. Corrensite was also found in the SDZ and, based on

composition, is likely to have a strength of $0.05 < \mu < 0.4$. Thus, corrensite along with increased quartz content (Supplementary Fig. 2) may be responsible for the marginally stronger frictional strength of the SDZ. Serpentine and minor amounts of other phyllosilicates (including chlorite, illite and micas) are present in the foliated gouge and, when added to the stronger quartz, feldspar and calcite constituents, result in a matrix strength that is consistent with estimates suggested by mixing law studies^{11–13}. Rock fabric that localizes weak minerals can lower frictional strength relative to the strength of ground and mixed samples¹⁴. Thus, the SAFOD foliated gouge may be even weaker in its undisturbed state than the values reported here.

Shear strength of fault gouge material typically varies with sliding rate. Rate dependence can be important in determining deformation mode (stable or unstable) and in extrapolating shear strength to SAF deformation rates. Steady-state rate sensitivity is defined¹⁵ by the parameter $(a - b) = d\mu_{ss}/d\ln V$, where μ_{ss} is the steady-state friction coefficient at velocity V . Imposed velocity steps, as shown in Fig. 2, are used to determine $a - b$. Negative values promote unstable slip, whereas positive values are likely to result in stable creep. The serpentinite porphyroclast from the SDZ shows a range of both negative and positive values ($a - b = +0.0004 \pm 0.0014$) similar to past values reported for serpentinites^{16,17}. All other core samples have positive rate sensitivity. Samples taken from outside the foliated gouge zones have values in the range $+0.001 < a - b < +0.007$. For CDZ, the combined measurements resulted in $a - b = +0.0018 \pm 0.0008$. For SDZ, values are twice as large: $a - b = +0.0037 \pm 0.0007$.

Average *in situ* strengths for CDZ and SDZ gouges (Fig. 1) are $\mu = 0.16$ and 0.19 , respectively. These measurements are determined for a slip rate of $1.15 \mu\text{m s}^{-1}$ ($36,000 \text{ mm yr}^{-1}$) and should be reduced to the appropriate *in situ* deformation rate ($\leq 34 \text{ mm yr}^{-1}$) of the SAF. (Note that the slowest imposed deformation rate in the strength tests ($0.0115 \mu\text{m s}^{-1}$, Fig. 2) is only about 11 times the *in situ* rate.) Extrapolation of test strengths using the observed rate sensitivity for the foliated gouge indicates upper bounds for steady-state strength of CDZ and SDZ, respectively, of $\mu = 0.14$ and 0.16 . This scaling assumes that the slip rate across the 1-mm-thick test gouge layer should be compared to the SAF deformation rate that is accommodated by the combined thickness of the SDZ and CDZ ($\sim 4.2 \text{ m}$). Depending on how strain is partitioned within the shear zones, the actual *in situ* shear strength supported by the deforming zones could be much less.

Although the SAF is one of the most well-studied fault systems in the world, fundamental questions about its strength and mechanical properties remain unanswered¹⁸. The SAF heat flow paradox was identified more than 40 years ago and is debated to this day^{19–23}. Essentially, if the shear strength of the SAF were consistent with common laboratory-derived Byerlee rock friction ($\mu > 0.6$), frictional heating of the fault during earthquakes and stable fault creep should result in increased temperature and heat flow adjacent to the fault zone. In addition, the maximum horizontal stress near the fault should be oriented at $\sim 30^\circ$ to the fault trace. However, no evidence of a heat-flow anomaly along the creeping section of the SAF has been found^{20,24}, and borehole stress observations at SAFOD confirm that the maximum horizontal stress at this locality is at a high angle to the fault trace^{4,5,25}. Although formation fluid pressure is apparently above hydrostatic in the sedimentary sequence northeast of the fault, there is no evidence from SAFOD drilling operations that pore pressure within the fault zone is elevated relative to the country rock¹. The direct measurement, reported here, of low frictional strength ($\mu \approx 0.15$) of foliated gouge material taken at depth from the actively deforming shear zones is consistent with both the lack of an observed heat flow anomaly and the maximum compressive stress oriented at a high angle to the fault trace. Also, the positive dependence of strength on slip rate of the fault gouge material is consistent with deformation by creep rather than by earthquakes.

Saponite becomes unstable above about 150°C (ref. 26) and is unlikely to be found deeper in the fault zone than 3.5–4 km (observed

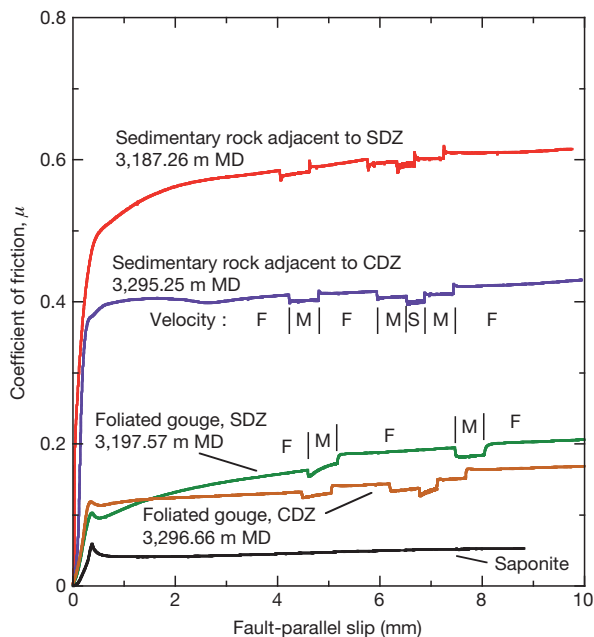


Figure 2 | Four representative deformation tests of core material from Hole G, with saponite for comparison. Periodic strength steps are due to decade changes in sliding rate (fault velocity in $\mu\text{m s}^{-1}$: fast (F), 1.15; medium (M), 0.115; slow (S), 0.0115). Strength variations are attributed to compositional differences between samples as shown in XRD patterns. Bottom curve shows strength of monomineralic saponite gouge taken from vesicles in altered volcanic rocks from the Isle of Skye, Scotland (obtained from Mineralogical Research Co.). Permanent strengthening during some slow velocity steps is the result of time-dependent compaction. Foliated gouge is 3–4 times stronger than pure saponite owing to the presence of strong minerals like quartz. MD, measured depth.

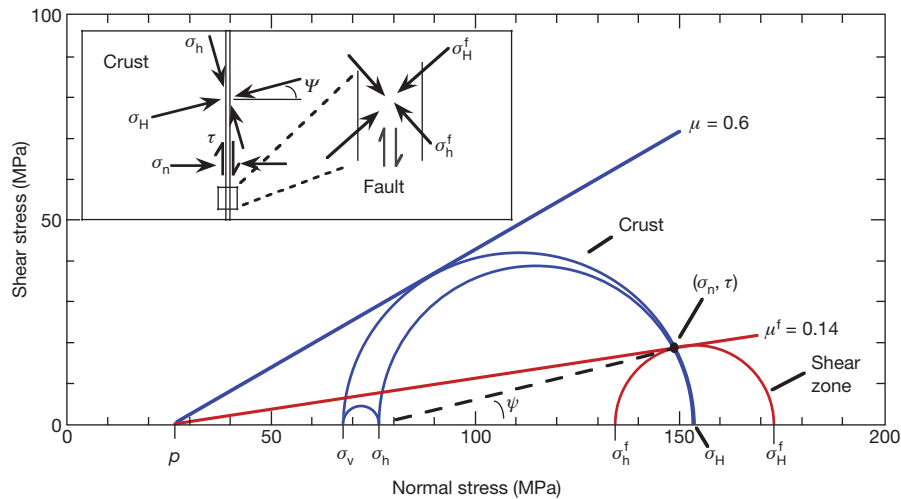


Figure 3 | Stress state for SAFOD drill site at 2.7 km depth. Model is based on borehole observations (assuming hydrostatic pore pressure) and foliated gouge strength (blue, host rock; red, weak shear zone). Main panel shows relationship of stress states within and outside the weak shear zone. Inset shows the corresponding spatial orientation of horizontal stresses in the model. While

temperature within the fault at ~ 2.7 km depth at SAFOD was 110–115 °C; C. Williams, personal communication). Stable creep and low strength of the deep SAF in the creeping section may reflect the presence of other low-strength minerals, elevated fluid pressure, or enhanced chemical weakening at greater depth than penetrated by SAFOD. Still, when considering the mechanics of the SAF specifically at 2.7 km, at SAFOD, mineralogy alone appears sufficient to explain fault strength.

Rice²⁷ analysed the stress state of a weak fault (due to elevated pore pressure, p) embedded in a stronger crust in a transpressional regime. Tembe *et al.*²⁸ extended the Rice analysis to include fault gouge of arbitrary strength. We use σ_H and σ_h for maximum and minimum horizontal principal stresses, respectively, and denote values within the fault by a superscript 'f'. Following Tembe *et al.*, a stress diagram representative of the SAFOD site at 2.7 km depth, with $\mu^f = 0.14$, $\mu = 0.60$ and hydrostatic p , is shown in Fig. 3. The model requires that σ_H (outside the weak shear zones) makes an angle of 77° to the strike of the SAF and is consistent with borehole observations at SAFOD showing high differential stresses in a transitional strike-slip to reverse-faulting stress regime, with σ_H maintaining a high angle to the SAF ($70\text{--}80^\circ$) at depth^{4,5}. Traction on the fault, in this model, are $\tau = 17$ MPa and $\bar{\sigma}_n = 122$ MPa.

SAFOD phase 3 drilling has provided, for the first time, continuous core samples from the actively deforming SAF at a depth of 2.7 km. A self-consistent picture is emerging about the strength and deformation processes of this complex portion of the SAF that represents the transition from locked to creeping portions of the fault. Measurements of frictional strength of core material from within the SAF damage zone show two low-strength ($\mu \approx 0.15$) foliated gouge zones that are 1.6 and 2.6 m wide. These zones correspond to the actively creeping shear zones that were independently identified by casing deformation within the phase 2 hole. These shear zones are embedded in stronger material with $\mu \approx 0.35\text{--}0.65$. The extremely low strength of the foliated gouge in an otherwise strong crust is sufficient to explain the observed orientation of maximum compressive stress at a high angle relative to the strike of the fault (Fig. 3) without invoking high fluid pressure or other proposed fault-weakening mechanisms.

METHODS SUMMARY

We measured frictional strength of 25 samples obtained from the SAFOD phase 3 Hole G core, composed of material that could be carved from the core or removed as chips or rubble. Some portions of the rock mass bounding the shear zones had sufficient cohesion to be sampled as solid mini-cores or prisms and will be reported on later. Samples were ground to a powder (<150 μm diameter) and

maximum shear stress in host rock is high, principal stresses rotate within the shear zone to accommodate the weaker material. In the fault, mean stress is high but shear stress is low. In model: $\sigma_H = 153$ MPa; $\sigma_h = 76$; $\sigma_v = 67.5$; $p = 27$. See text for definitions of symbols used.

sheared in 1- or 2-mm-thick gouge layers between 25.4-mm-diameter driving blocks in a triaxial deformation apparatus¹³ (Supplementary Fig. 1). Most samples were saturated with brine equivalent to *in situ* pore fluid (Y. Kharaka and J. Thordsen, personal communication) at 1 MPa constant pore pressure; a few tests were conducted with deionized water. Tests were performed at room temperature, constant effective normal stress (40, 120 and 200 MPa) and constant sliding rate (0.0115, 0.115 and 1.15 $\mu\text{m s}^{-1}$). Tests were carried out to 200 MPa to be applicable to *in situ* stress conditions (Fig. 3) and to allow for interpolation to other depths.

Full Methods and any associated references are available in the online version of the paper at www.nature.com/nature.

Received 19 October 2010; accepted 31 January 2011.

Published online 23 March 2011.

- Zoback, M., Hickman, S. & Ellsworth, W. Scientific drilling into the San Andreas Fault zone. *Eos* **91**, 197–199 (2010).
- Moore, D. E. & Rymer, M. J. Talc-bearing serpentinite, and the creeping section of the San Andreas fault. *Nature* **448**, 795–797 (2007).
- Moore, D. E. & Rymer, M. J. Metasomatic origin of fault gouge comprising the two creeping strands at SAFOD. *Eos* (Fall suppl.), paper T41A-2105 (2010).
- Boness, N. & Zoback, M. D. A multi-scale study of the mechanisms controlling shear velocity anisotropy in the San Andreas Fault Observatory at Depth. *Geophysics* **71**, F131–F146 (2006).
- Hickman, S. & Zoback, M. D. Stress measurements in the SAFOD pilot hole: implications for the frictional strength of the San Andreas fault. *Geophys. Res. Lett.* **31**, L15S12, doi:10.1029/2004GL020043 (2004).
- Zoback, M. D., Hickman, S. & Ellsworth, W. in *Treatise on Geophysics* Vol. 4 (ed. Schubert, G.) 649–674 (Elsevier, 2007).
- Tobin, H., Ito, H., Behrmann, J., Hickman, S. H. & Kimura, G. in *Report from IODP/ICDP Workshop on Fault Zone Drilling, Scientific Drilling* (eds Ito, H. *et al.*) 5–16 (Special Issue No. 1, Integrated Ocean Drilling Program, Hokkaido, 2007).
- Solum, J. G. *et al.* Mineralogical characterization of protolith and fault rocks from the SAFOD main hole. *Geophys. Res. Lett.* **33**, L21314, doi:10.1029/2006GL027285 (2006).
- Tembe, S. *et al.* Frictional strength of cuttings and core from SAFOD drillhole phases 1 and 2. *Geophys. Res. Lett.* **33**, L23307, doi:10.1029/2006GL027626 (2006).
- Holdsworth, R. E. *et al.* Fault rocks from the SAFOD core samples: implications for weakening at shallow depths along the San Andreas Fault, California. *J. Struct. Geol.* **33**, 132–134 (2011).
- Moore, D. E. & Lockner, D. A. Frictional strengths of talc-serpentinite and talc-quartz mixtures. *J. Geophys. Res.* **116**, B01403, doi:10.1029/2010JB007881 (2011).
- Crawford, B. R., Faulkner, D. R. & Rutter, E. H. Strength, porosity, and permeability development during hydrostatic and shear loading of synthetic quartz-clay fault gouge. *J. Geophys. Res.* **113**, B03207, doi:10.1029/2006JB004634 (2008).
- Tembe, S., Lockner, D. A. & Wong, T.-f. Effect of clay content and mineralogy on frictional sliding behavior of simulated gouges: binary and ternary mixtures of quartz, illite and montmorillonite. *J. Geophys. Res.* **115**, B03416, doi:10.1029/2009JB006383 (2010).
- Colletini, C., Niemeijer, A., Viti, C. & Marone, C. Fault zone fabric and fault weakness. *Nature* **462**, 907–910 (2009).
- Dieterich, J. H. Modeling of rock friction 1. Experimental results and constitutive equations. *J. Geophys. Res.* **84**, 2161–2168 (1979).

16. Moore, D. E., Lockner, D. A., Ma, S., Summers, R. & Byerlee, J. D. Strengths of serpentinite gouges at elevated temperatures. *J. Geophys. Res.* **102**, 14787–14801 (1997).
17. Moore, D. E., Lockner, D. A., Tanaka, H. & Iwata, K. The coefficient of friction of chrysotile gouge at seismogenic depths. *Int. Geol. Rev.* **46**, 385–398 (2004).
18. Hickman, S. H. Stress in the lithosphere and the strength of active faults. *Rev. Geophys.* **29**, 759–775 (1991).
19. Brune, J. N., Henyey, T. L. & Roy, R. F. Heat flow, stress, and rate of slip along the San Andreas fault, California. *J. Geophys. Res.* **74**, 3821–3827 (1969).
20. Lachenbruch, A. H. & Sass, J. H. Heat flow and energetics of the San Andreas fault zone. *J. Geophys. Res.* **85**, 6185–6222 (1980).
21. Scholz, C. H. Evidence for a strong San Andreas fault. *Geology* **28**, 163–166 (2000).
22. Zoback, M. D. Strength of the San Andreas. *Nature* **405**, 31–32 (2000).
23. Saffer, D. M., Bekins, B. A. & Hickman, S. Topographically driven groundwater flow and the San Andreas heat flow paradox revisited. *J. Geophys. Res.* **108**, 2274, doi:10.1029/2002JB001849 (2003).
24. Lachenbruch, A. H. & Sass, J. H. Heat flow from Cajon Pass, fault strength, and tectonic implications. *J. Geophys. Res.* **97**, 4995–5015 (1992).
25. Zoback, M. D. *et al.* New evidence on the state of stress of the San Andreas fault system. *Science* **238**, 1105–1111 (1987).
26. Inoue, A. & Utada, M. Smectite-to-chlorite transformation in thermally metamorphosed volcanoclastic rocks in the Kamikita area, northern Honshu, Japan. *Am. Mineral.* **76**, 628–640 (1991).
27. Rice, J. R. in *Fault Mechanics and Transport Properties of Rocks* (eds Evans, B. & Wong, T.-f.) 475–503 (Academic, 1992).
28. Tembe, S., Lockner, D. & Wong, T.-f. Constraints on the stress state of the San Andreas fault with analysis based on core and cuttings from San Andreas Observatory at Depth (SAFOD) drilling phases 1 and 2. *J. Geophys. Res.* **114**, B11401, doi:10.1029/2008JB005883 (2009).

Supplementary Information is linked to the online version of the paper at www.nature.com/nature.

Acknowledgements We thank B. Weymer, J. Firth and P. Nelson for their assistance and patience in providing the core material. Comments from W. Ellsworth, D. Faulkner and R. Simpson significantly improved the manuscript.

Author Contributions C.M. and D.A.L. conducted deformation experiments, D.M. provided petrographic analysis and XRD measurements, and S.H. provided borehole logging results and related stress analysis.

Author Information Reprints and permissions information is available at www.nature.com/reprints. The authors declare no competing financial interests. Readers are welcome to comment on the online version of this article at www.nature.com/nature. Correspondence and requests for materials should be addressed to D.A.L. (dlockner@usgs.gov).

METHODS

Sample preparation. We measured frictional strength of 25 samples that were obtained from the SAFOD phase 3 Hole G core. Hole G was cored in measured depth intervals 3,186.7–3,199.5 m and 3,294.9–3,312.7 m to sample localized shear zones within the SAF damage zone that correspond to the two intervals, referred to as SDZ and CDZ, where slow deformation was observed in the Phase 2 casing¹. As indicated in Fig. 1, the cored intervals in Hole G were within or adjacent to the SAF damage zone as determined by logging data following phase 2 drilling. While selected samples were obtained to provide whole, undisturbed wafers for intact strength tests, samples tested here were either carved from the core or collected as rubble, chips or loose powder. All samples reported here were prepared by repeated gentle grinding with mortar and pestle until all material passed through a 100 mesh sieve (0.15 mm diameter). Resulting powder was then wetted to make a paste that was formed into a 1-mm-thick test layer (2-mm layers were used in the 200 MPa tests). The first 14 tests were performed with deionized water. All remaining tests used a prepared brine solution that duplicates the major cations and their relative concentrations found in the formation fluid retrieved from the SAFOD drill hole on the northeastern side of the SAF (Y. Kharaka and J. Thordsen, personal communication). Test fluid constituents, expressed in units of grams per litre, are: Cl^- , 13.32; Na^+ , 5.34; Ca^{2+} , 2.77; and K^+ , 0.22. Comparison tests showed only a slight difference between frictional strength for samples sheared with deionized water and samples sheared with the brine solution. Before mechanical testing, X-ray diffraction patterns were obtained to determine mineral composition and relative abundance.

Testing details. Tests were performed in a standard triaxial apparatus at room temperature and effective normal stresses of 40, 120 and 200 MPa. A constant pore pressure of 1 MPa was applied in all tests. Samples were 25.4-mm-diameter right-cylinders that contained a sawcut inclined 30° to the sample axis (Supplementary Fig. 1). The sawcut forcing blocks were sandstone–sandstone, sandstone–granite, or granite–granite pairs. Surfaces of forcing blocks were roughened with 100 grit abrasive, to assure good frictional contact with the applied gouge layer. See, for example, refs 9 and 13 for details. Berea sandstone forcing blocks have high permeability but also have 20% porosity that decreases with applied load. The standard test geometry used Berea for the top forcing block to assure rapid hydraulic communication of the fault with the external pore fluid system. Pore fluid flow in and out of the lower driving block was through the fault gouge. To minimize pore pressure transients due to stress changes, low-porosity granite was

used for the lower driving block in most tests, and particularly in experiments with low-permeability clay-rich gouge.

A greased Teflon shim, placed between the piston and the sample assembly, allowed easy lateral slip of the lower driving block during shearing (Supplementary Fig. 1). Samples were jacketed in 3.2-mm-thick latex tubing for isolation from confining fluid. Separate calibration tests showed that the latex tubing provided an equivalent shear resistance of 0.043 MPa mm⁻¹ due to stretching during deformation experiments. This shear strength correction has been applied to all test results. Shear and normal stresses have also been corrected for the reduction in contact area as the two sample halves slide past each other¹³. Axial load was measured with an internal load cell. Axial shortening, confining pressure and pore pressure were all measured at 1-s intervals. Shear and normal stress resolved on the fault surface were computed in real time from the axial stress, confining pressure and axial shortening. As sample strength varied, confining pressure was adjusted every second to maintain constant normal stress. Axial stress, confining pressure and pore pressure have accuracies of at least 0.03 MPa. Samples were sheared to 9 mm axial shortening (~10.4 mm parallel to the sawcut) at axial shortening rates of 0.01, 0.1 and 1.0 $\mu\text{m s}^{-1}$ to determine the dependence of shear strength on sliding rate and thereby the tendency for stable creep or unstable slip. Slip and slip rate on the inclined fault surfaces were 15% higher than the corresponding axial values. Steady-state changes in strength were estimated for individual velocity steps by measuring the residual strength change after de-trending the friction–displacement curves for long-term strain hardening. This procedure was carried out manually.

Measurement accuracy. Sample strength is reported as coefficient of friction $\mu = \tau/\bar{\sigma}_n$. Within a single experiment, changes in μ have a precision of ± 0.001 . Reproducibility of μ between experiments, including variations due to sample preparation, is approximately ± 0.005 . Accuracy of μ , after corrections for true contact area and jacket strength, is approximately ± 0.01 . Initial gouge layer thickness is 1.0 mm for 40 and 120 MPa tests. Gouge layer thickness is 2.0 mm for 200 MPa tests to offset thinning at the higher normal stress. Compaction is not measured during experiments, but layer thickness following experiments is reduced by 5–30%, depending on normal stress, gouge clay content and driving block type. As shear will localize within the gouge layer to different degrees and at different times, depending on composition and normal stress, estimates of true shear strain are problematic. The deformation quantity that is most accurately determined in these experiments is total fault-parallel slip. This can be converted to a nominal shear strain by dividing by the initial 1 or 2 mm gouge thickness.